

Influence of Dynamical Pauli Effect and Dynamical Symmetry Breaking to Quantum Chaos

Ming-Tsung Lee^a, Wei-Min Zhang^b and Cheng-Li Wu^c

^a*Department of Physics, National Taiwan University, Taipei 107, Taiwan, ROC*

^b*Institute of Physics, Academia Sinica, Taipei 115, Taiwan, ROC*

^c*Department of Physics, Chung-Yuan Christian University, Chung Li 320, Taiwan, ROC*

(Oct. 22, 1997)

Abstract

In this paper, we study the influence of quantum effects to chaotic dynamics, especially the influence of Pauli effect and dynamical symmetry breaking to chaotic motions. We apply the semiquantal theory to the $Sp(6)$ fermion symmetry model in nuclear collective motion. We demonstrate that quantum chaos appears when dynamical symmetry is broken. We further show that dynamical Pauli effect enhances quantum chaos.

PACS: 05.45.+b, 21.60.-n, 24.60.Lz, 03.65.Sq

I. INTRODUCTION

Quantum chaos is one of the most challenge research topics in both theoretical and experimental physics. In the past decade, in order to understand the concept of quantum chaos, people have been focusing on seeking the generic behavior in quantum spectra and wave functions of various dynamical systems whose classical dynamics are chaotic. In these investigations, two significant features have been found. One of them is the relation between the quantum energy level statistical distributions of the classical chaotic systems and the GOE/GUE spectral statistical universality classes of the random matrix theory [1]. The

other feature is the existence of “scars” in individual eigenstate wave functions, i.e., the appearance of strong localization of wave functions along the unstable periodic orbits in chaotic systems [2]. However, the dynamical mechanism of quantum manifestation of chaos is still not well understood so far.

In order to study the dynamical mechanism of quantum manifestation of chaos, one of us developed an approach, called the semiquantal approach [3]. The main motivation of this approach is to provide a framework to study how quantum fluctuations, quantum correlations and other quantum phenomena manifest themselves in the classical trajectories. This approach differs from the above mentioned investigations. It starts from quantum systems without reference to classical limit and it directly explores the dynamics of quantum effects in classical chaotic trajectories. Therefore, it provides a systematic way to explore the intrinsic mechanism of quantum manifestation of chaos [4–8].

The general theoretical framework of the semiquantal approach is the stationary phase approximation of the generalized coherent state path integral [9]. Each set of generalized coherent states associated with the dynamical group G of a quantum system forms an over-complete set of states for an irreducible representation space of G . The coherent states are also in one-to-one corresponding to a geometrical space which has a symplectic structure. We called this geometrical space the quantum phase space. Based on path integral formulation, coherent states then embed each quantum system in a quantum phase space, regardless of whether the system has a classical counterpart or not. The stationary phase approximation further results in a set of dynamical equations of motion on this quantum phase space, which are similar to the classical equations of motion. But the Hamiltonian function governed these dynamical equations of motion is the expectation values of the Hamiltonian operator in the generalized coherent states, which contain the leading quantum fluctuations and correlations. We called these equations of motion the semiquantal dynamical equations. This formulation allows us to directly explore the dynamical effects of quantum fluctuations and correlations to chaos [3].

Based on this formulation of semiquantal dynamics, we will study in this paper the

dynamical effect of the Pauli exclusive principle to chaotic motions. We shall take the $\text{Sp}(6)$ model, the $\text{Sp}(6)$ symmetry of the fermion dynamical symmetry model in nuclear many-body systems [11], as our example. This model is a microscopic description of nuclear collective dynamics with fermions as the building blocks. A significant feature of this model is that the Pauli principle of fermions has a crucial influence on the low-lying nuclear collective modes, which manifests themselves in experimental data [12]. When we define a set of canonical deformation variables (the quantum phase space) associated with the $\text{Sp}(6)$ coherent states, the connection between Bohr-Mottelson geometrical model [13] and the $\text{Sp}(6)$ model can be built [14]. The Pauli effect in the $\text{Sp}(6)$ model itself manifests in the nuclear deformation in terms of some constraints on the nuclear surface (deformation) variables [15]. Within the semiclassical framework, the Poincaré's picture of chaos can be applied to describe the possible chaotic dynamics in nuclear collective motion in the aforementioned quantum phase space. Therefore, dynamical Pauli effect to chaos can be explicitly studied. Our result shows that dynamical Pauli effect enhances the pairing correlations (quantum correlation) and inhibits nuclear deformation. This gives rise to the breaking of dynamical symmetry and therefore leads to the occurrence of chaos.

The paper is organized as follows: In Sec. 2, the nuclear shape in terms of the microscopic fermion degrees of freedom is parameterized through the $\text{Sp}(6)$ coherent states. The coherent state of the $\text{Sp}(6)$ model in the nuclear body frame is constructed so that the quantum phase space of the $\text{Sp}(6)$ model is connected with the nuclear geometrical model. In Sec. 3, the semiclassical dynamical equations of motion for nuclear deformation is derived. With the consideration of time-reversal invariance and valence nucleon number conservation, the resulting equations of motion are reduced to a set of Hamilton-like equations in a four-dimensional quantum phase space, which describes the nuclear surface motions. In Sec. 4, we explore the geometrical manifestation of dynamical Pauli effect and numerically examine the dynamical effect of the Pauli principle and dynamical symmetry breaking in semiclassical framework, from which we find that quantum chaos appears when dynamical symmetry is broken and dynamical Pauli effect enhances quantum chaos. Finally, a summary is presented

in Sec. 5.

II. PHASE SPACE PARAMETERIZATION OF NUCLEAR SHAPE AND GEOMETRICAL INTERPRETATION

We begin with the fermion dynamical symmetry Sp(6) model [11] which describe the nuclear collective motions. The Sp(6) group is spanned by the collective pairing operators $\{\hat{S}, \hat{D}_\mu\}$ and the collective particle-hole quadrupole operators $\{\hat{P}_{\lambda\mu}; \lambda = 0, 1, 2; \mu = -\lambda, \dots, \lambda\}$. The model Hamiltonian operator is given by

$$\hat{H} = \epsilon \hat{n} + G_0 \hat{S}^+ \hat{S} + \sum_{l=1,2} b_l \hat{P}_l \cdot \hat{P}_l, \quad (1)$$

where \hat{n} is the particle number operator. The coefficient ϵ, G_0 and b_l represent the strength of the internal energy, effective pairing and multiple interactions, respectively. It is worth noticing that the D -pairing interactions are not included in Eq. (1) because such interactions can be replaced by the S -pairing and multiple interactions in the Sp(6) symmetry [11]. Also, in order to study chaotic dynamics of nuclear deformation under the Sp(6) model, we should only consider the dynamics of different intrinsic bands rather than the collective motion within a single band. Therefore, we can let $b_1 = b_2$ in Eq. (1).

To study the nuclear surface motions in the Sp(6) model within the semiquantal framework, one must first construct the corresponding quantum phase space. It has been shown that such a quantum phase space is uniquely realized by the coset space $\text{USp}(6)/\text{U}(3)$ through the Sp(6) coherent states. (The detailed construction of the coherent states of the Sp(6) model can be found in Ref. [14]. It has also been roughly summarized in Appendix A.)

In the following subsections, we will parametrize the nuclear shape in the above mentioned quantum phase space by visualizing nuclear deformation to be a geometrical description of the microscopic Sp(6) fermion model. As it is well-known, the dynamics of nuclear deformation has time reversal invariance. Meantime, it is also convenient to describe nu-

clear deformation in the nuclear intrinsic frame in which adequate deformed variables can be chosen as the coordinates of the $\text{Sp}(6)$ quantum phase space.

A. The time reversal invariant deformed coherent states

First, we shall look at the connection of the $\text{Sp}(6)$ Coherent States (CS) with nuclear deformation. In the macroscopic picture of the nuclear geometrical model, the rotational and vibrational energy spectrum of nuclei are described in according to the nuclear surface motions. The nuclear surface can be defined by

$$R(t, \theta, \phi) = R_0 \left(\sum_{\lambda=0,1,2, \mu=-\lambda, \dots, \lambda} \alpha_{\lambda\mu}^*(t) Y_{\lambda\mu}(\theta, \phi) \right) + R_c, \quad (2)$$

where R_0 is the maximum thickness of a nucleus, R_c the radius of frozen core, and $Y_{\lambda\mu}(\theta, \phi)$ the spherical harmonic function. In Eq. (2), the quadrupole terms (with $\lambda = 2$) play the dominant role in the description of nuclear deformation. They determine the strength of nuclear surface motions. The monopole term ($\lambda = 0$) describes the shell thickness of the undeformed compressible nucleus. When the center of nuclei is fixed in a reference frame (no translation), the effect of $\lambda = 1$ term can be ignored. Besides, all the surface variables in Eq. (2) satisfy the time reversal symmetry so that

$$\alpha_{\lambda\mu}^*(t) = (-1)^\mu \alpha_{\lambda-\mu}(t). \quad (3)$$

To generalize this concept into the framework of a microscopic description, we introduce a deformation matrix ρ ,

$$\rho = - \left(\alpha_{00}(t) \mathbf{I}_{3 \times 3} + 2 \sum_{\mu=-2}^2 \alpha_{2\mu}^*(t) \mathbf{P}_{2\mu} \right), \quad (4)$$

which is related to the quadrupole momentum in the $\text{Sp}(6)$ model, where $\mathbf{I}_{3 \times 3}$ is a 3×3 identity matrix; and $\mathbf{P}_{2\mu}$ the submatrix block of the quadrupole momentum operator $\hat{P}_{2\mu}$ in the 6×6 matrix representation of the $\text{Sp}(6)$ group. The detailed expressions can be found in Appendix A of Ref. [14]. These submatrices $\mathbf{P}_{\lambda\mu}$ form an irreducible representation of the

unitary subgroup $U(3)$. They determine the deformation properties of nucleus. The surface variables $\alpha_{\lambda\mu}$ still obey the time reversal invariance condition (3), and the coefficient $\alpha_{00}(t)$ is chosen to be negative. This is because the shell thickness of the undeformed nucleus is positive, and also the quadrupole momentum must also be positive when the particle number is less than Ω , where Ω is the pair degeneracy of normal-parity levels in a major shell (i.e. Ω_1 in the $Sp(6)$ model). In this paper we only consider the case of valence particle number $n \leq \Omega$. For the case $n > \Omega$, an analogous discussion can be made because of the particle-hole symmetry.

Next, we shall build the connection between the surface variables $\alpha_{\lambda\mu}(t)$ and the parameters in the $Sp(6)$ coherent states. As one can find in Ref. [14] (also see Appendix A), the $Sp(6)$ coherent state $|\eta\rangle$ is completely determined by a 3×3 parameter matrix \mathbf{X} . Meantime, the 3×3 hermitian matrix $\sqrt{\mathbf{X}\mathbf{X}^+}$ can be spanned by $\mathbf{P}_{2\mu}$:

$$\sqrt{\mathbf{X}\mathbf{X}^+} = \sum_{\lambda=0,2,\mu=-\lambda,\dots,\lambda} \beta_{\lambda\mu}^*(\chi_{\lambda'\mu'}(t)) \mathbf{P}_{\lambda\mu}, \quad (5)$$

where $\mathbf{P}_{\lambda\mu}$ obey the condition: $\mathbf{P}_{\lambda-\mu} = (-1)^\mu \mathbf{P}_{\lambda\mu}^\dagger$. Furthermore, the hermitian property of the matrix $\sqrt{\mathbf{X}\mathbf{X}^+}$ implies that

$$\beta_{\lambda-\mu}^* = (-1)^\mu \beta_{\lambda\mu} \quad (6)$$

which corresponds to the time reversal invariance.

Without any loss of generality, we can set the matrix $\sqrt{\mathbf{X}\mathbf{X}^+}$ to be equal to the deformation matrix ρ by letting $\beta_{\lambda\mu}(t) = (-1)^\mu \alpha_{\lambda\mu}(t)$. The connection between the surface variables $\alpha_{\lambda\mu}(t)$ and the coherent state parameters in $|\eta\rangle$ can then be carried out. The properties of nuclear deformation determined by the $Sp(6)$ CS are described by Eqs. (3-4) and the requirement $\sqrt{\mathbf{X}\mathbf{X}^+} \equiv \rho$. The explicit form of the matrix $\sqrt{\mathbf{X}\mathbf{X}^+}$ is given as

$$\sqrt{\mathbf{X}\mathbf{X}^+} \equiv \rho = - \begin{bmatrix} \alpha_{00} + \sqrt{\frac{1}{2}}\alpha_{20} & \sqrt{\frac{3}{2}}\alpha_{21}^* & \sqrt{3}\alpha_{22}^* \\ \sqrt{\frac{3}{2}}\alpha_{21} & \alpha_{00} - \sqrt{2}\alpha_{20} & -\sqrt{\frac{3}{2}}\alpha_{21}^* \\ \sqrt{3}\alpha_{22} & -\sqrt{\frac{3}{2}}\alpha_{21} & \alpha_{00} + \sqrt{\frac{1}{2}}\alpha_{20} \end{bmatrix}. \quad (7)$$

B. The deformed coherent states in the intrinsic frame (ICS)

In order to make the dynamics of nuclear deformation manifestation, it is convenient to express the nuclear deformation parameters in the nuclear intrinsic frame (i.e. the nuclear body frame). We call the CS describing the nuclear deformation in the nuclear intrinsic frame the intrinsic coherent states (ICS). In the intrinsic frame, the deformation matrix is positive and diagonal. To deduce the ICS, a basic idea is to decompose the previous spherical tensor operators into proper cartesian tensor operators.

The cartesian tensor operator \hat{a}_{ij} are defined as follows:

$$\hat{a}_{ij} = \sum_{lm=1,2,3} (U_{il} \hat{B}_{lm} U_{mj}^+) \quad , \quad i, j = 1, 2, 3, \quad (8)$$

where the index $1 \rightarrow x, 2 \rightarrow z, 3 \rightarrow y$ for \hat{a}_{ij} . Such an index assignment corresponds to a choice of the left-hand coordinate system in order to be consistent with the notations used in Ref. [14]. The operators \hat{B}_{lm} are uncoupled particle-hole operators in the Sp(6) model. The connection between \hat{B}_{lm} and $\hat{P}_{\lambda\mu}$ can be found in Ref. [14]. The transformation matrix U is defined by:

$$U = \frac{1}{\sqrt{2}} \begin{bmatrix} 1 & 0 & -1 \\ 0 & \sqrt{2} & 0 \\ -i & 0 & -i \end{bmatrix}. \quad (9)$$

With the above cartesian tensor operators, the rank-one spherical tensor operators can be expressed in terms of \hat{a}_{ij} ,

$$\begin{aligned} \hat{P}_{11} &= \frac{\sqrt{3}}{4} (\hat{a}_{zx} - \hat{a}_{xz} + i \hat{a}_{zy} - i \hat{a}_{yz}), \\ \hat{P}_{1-1} &= \frac{\sqrt{3}}{4} (\hat{a}_{zx} - \hat{a}_{xz} + i \hat{a}_{yz} - i \hat{a}_{zy}), \\ \hat{P}_{10} &= i \sqrt{\frac{3}{8}} (\hat{a}_{yx} - \hat{a}_{xy}), \end{aligned} \quad (10)$$

and the rank-two spherical tensor operators $\hat{P}_{2\mu}$ (quadrupole momentum operators),

$$\hat{P}_{20} = \sqrt{\frac{1}{8}} (\hat{a}_{xx} - 2\hat{a}_{zz} + \hat{a}_{yy}),$$

$$\begin{aligned}
\hat{P}_{21} &= -\frac{\sqrt{3}}{4} (\hat{a}_{zx} + \hat{a}_{xz} + i \hat{a}_{yz} + i \hat{a}_{zy}) , \\
\hat{P}_{2-1} &= \frac{\sqrt{3}}{4} (\hat{a}_{zx} + \hat{a}_{xz} - i \hat{a}_{yz} - i \hat{a}_{zy}) , \\
\hat{P}_{22} &= \frac{\sqrt{3}}{4} (-\hat{a}_{xx} + \hat{a}_{yy} - i \hat{a}_{xy} - i \hat{a}_{yx}) , \\
\hat{P}_{2-2} &= \frac{\sqrt{3}}{4} (-\hat{a}_{xx} + \hat{a}_{yy} + i \hat{a}_{xy} + i \hat{a}_{yx}) .
\end{aligned} \tag{11}$$

Let us now consider the matrix representation in terms of \hat{a}_{ij} as the basis,

$$\hat{a}_{ij} \longrightarrow \text{Rep}(\hat{a}_{ij}) = e_{ij} = \begin{bmatrix} E_{ij} & 0 \\ 0 & -E_{ji} \end{bmatrix} , \tag{12}$$

where E_{ij} is a 3×3 matrix with +1 in the i -th row and the j -th column, and zero everywhere else. The deformation matrix ρ in this cartesian basis is then expressed as

$$\rho = - \begin{bmatrix} \alpha_{00} + \sqrt{\frac{1}{2}}\alpha_{20} & \sqrt{\frac{3}{4}}(\alpha_{21} + \alpha_{21}^*) & i\sqrt{\frac{3}{4}}(\alpha_{22} - \alpha_{22}^*) \\ -\sqrt{\frac{3}{4}}(\alpha_{22} + \alpha_{22}^*) & \alpha_{00} - \sqrt{2}\alpha_{20} & -i\sqrt{\frac{3}{4}}(\alpha_{21} - \alpha_{21}^*) \\ \sqrt{\frac{3}{4}}(\alpha_{21} + \alpha_{21}^*) & \alpha_{00} - \sqrt{2}\alpha_{20} & -i\sqrt{\frac{3}{4}}(\alpha_{21} - \alpha_{21}^*) \\ i\sqrt{\frac{3}{4}}(\alpha_{22} - \alpha_{22}^*) & i\sqrt{\frac{3}{4}}(\alpha_{21}^* - \alpha_{21}) & \alpha_{00} + \sqrt{\frac{1}{2}}\alpha_{20} \\ & & + \sqrt{\frac{3}{4}}(\alpha_{22} + \alpha_{22}^*) \end{bmatrix} , \tag{13}$$

where the parameters $\{\alpha_{\lambda\mu}\}$ maintain the tensorial structure under rotational transformation, i.e.

$$R^{-1}(\omega) \rho(\alpha_{\lambda\mu}) R(\omega) = \rho(\alpha'_{\lambda\nu}) , \tag{14}$$

and $\alpha'_{\lambda\nu}$ is given by

$$\alpha'_{\lambda\nu} = \sum_{\mu=-\lambda}^{\lambda} \alpha_{\lambda\mu} D_{\mu\nu}^{\lambda}(\omega) , \tag{15}$$

$$\alpha'_{\lambda\nu}^* = (-1)^{\nu} \alpha'_{\lambda-\nu} , \tag{16}$$

with $R(\omega)$ being a Euler rotational matrix, ω the Euler angular, and $D_{\mu\nu}^{\lambda}(\omega)$ the Wigner- D function. One can always find an Euler rotation $R(\omega)$ such that the nucleus is described in an intrinsic frame in which ρ is diagonal (i.e. $\alpha'_{21} = 0$ and α'_{22} is real):

$$\rho_{in} = \begin{bmatrix} |S_x| & 0 & 0 \\ 0 & |S_z| & 0 \\ 0 & 0 & |S_y| \end{bmatrix}. \quad (17)$$

Since $\rho_{in} = \sqrt{\mathbf{X}_{in}\mathbf{X}_{in}^+}$, the matrix \mathbf{X}_{in} (the Sp(6) CS parameter matrix in the intrinsic frame) can be chosen as:

$$\mathbf{X}_{in} = \begin{bmatrix} S_x & 0 & 0 \\ 0 & S_z & 0 \\ 0 & 0 & -S_y \end{bmatrix}. \quad (18)$$

The minus sign of S_y in the above equation is due to the use of the right hand coordinate system. The explicit form of the parameters S_i is given as follows,

$$\begin{aligned} S_x &= - \left(\alpha_{00} + \frac{1}{\sqrt{2}}\alpha_{20} - \sqrt{3}\alpha_{22} \right) e^{-if_x(\alpha_{00}, \alpha_{20}, \alpha_{22}; \pi_{00}, \pi_{20}, \pi_{22})}, \\ S_z &= \left(-\alpha_{00} + \sqrt{2}\alpha_{20} \right) e^{-if_z(\alpha_{00}, \alpha_{20}, \alpha_{22}; \pi_{00}, \pi_{20}, \pi_{22})}, \\ S_y &= - \left(\alpha_{00} + \frac{1}{\sqrt{2}}\alpha_{20} + \sqrt{3}\alpha_{22} \right) e^{-if_y(\alpha_{00}, \alpha_{20}, \alpha_{22}; \pi_{00}, \pi_{20}, \pi_{22})}, \end{aligned} \quad (19)$$

where the detailed functions of f_x , f_z and f_y can be found in Appendix C. In the intrinsic frame, the deformation degrees of freedom ($\sqrt{\mathbf{X}\mathbf{X}^+}$) are reduced to three because the intrinsic frame is chosen to be along the three principal axes of the nucleus. Together with the corresponding conjugate momentum variables, the phase space of nuclear deformation is a six-dimensional space. The six independent variables are now completely determined by the three complex parameters of \mathbf{X}_{in} in ICS.

Based on ICS, the nuclear deformation is described by the variables $|S_i|$ only. The physical picture of the variables $|S_i|$ can be seen from Eq. (2) which can be reexpressed in terms of cartesian coordinates as follows:

$$\begin{aligned} R(t, x, z, y) &= R_c + R_0 \left(|\alpha_{00}| + \alpha_{xx} \frac{x^2}{r^2} + \alpha_{yy} \frac{y^2}{r^2} + \alpha_{zz} \frac{z^2}{r^2} \right. \\ &\quad \left. + 2\alpha_{xz} \frac{xz}{r^2} + 2\alpha_{xy} \frac{xy}{r^2} + 2\alpha_{yz} \frac{yz}{r^2} \right), \end{aligned} \quad (20)$$

where $r = \sqrt{x^2 + z^2 + y^2}$. Since the intrinsic frame is chosen to be the three principal axes of nucleus in the intrinsic frame, the terms α_{xz} , α_{xy} and α_{yz} vanish. The deformation matrix then becomes:

$$\rho_{in} = -\alpha_{00}(t)\mathbf{I}_{3\times 3} + \sum_{i=x,y,z} \alpha_{ii}(t)\mathbf{A}_{ii}, \quad (21)$$

where \mathbf{A}_{ii} is the subblock matrix in the matrix representation of \hat{a}_{ij} , and

$$\alpha_{ii}(t) = \alpha_{00}(t) + |S_i(t)|. \quad (22)$$

According to Eq. (21), the length of the nucleus along the i th-axis is given by $R_0|S_i(t)| + R_c$. In other words, $\{S_i\}$ are the variables measuring nuclear deformation. These are exactly the dynamical variables we want to use to study the nuclear surface motions.

Once we have constructed the Sp(6) CS in the intrinsic frame, we can now derive the semiquantal dynamical equations of the nuclear collective motions.

III. THE SEMIQUANTAL DYNAMICS FOR SP(6) MODEL

The semiquantal dynamics of the Sp(6) model is determined by the time-dependent variational approach to the effective action (i.e. the stationary phase approximation of the generalized CS path integral):

$$S = \int dt \langle \text{ICS} | i\partial_t - \hat{H} | \text{ICS} \rangle. \quad (23)$$

The result of such a variation is a set of Hamilton-like equations

$$\begin{aligned} i\hbar \frac{\Omega}{3} \dot{S}_i^* &= -\frac{\partial \langle \hat{H} \rangle}{\partial S_i}, \\ i\hbar \frac{\Omega}{3} \dot{S}_i &= \frac{\partial \langle \hat{H} \rangle}{\partial S_i^*}, \quad , \quad i = x, y, z. \end{aligned} \quad (24)$$

These equations of motion are the semiquantal dynamical equations which approximately describe the quantum dynamics of nuclear deformation in the Sp(6) model. The word ‘‘approximately’’ (or semiquantal) means that this is an approximation of the Schödinger

equation described by the Hamilton-like equations of motion but it is derived purely from quantum mechanics. And the Hamiltonian function $\langle \hat{H} \rangle = \langle \text{ICS} | \hat{H} | \text{ICS} \rangle$ contains all the leading order quantum correlations. In nuclear many-body systems, this set of equations of motion is indeed the familiar time-dependent Hartree-Fock-Bogoliubov equations under the constraint of dynamical symmetry group $\text{Sp}(6)$ [15].

Note that Eq. (24) contains six equations of motion. However, not all these six equations of motions are independent. This is because for a given nucleus, the valence nucleon number is fixed:

$$n \equiv \langle \hat{n} \rangle = \frac{2\Omega}{3} (|S_x|^2 + |S_y|^2 + |S_z|^2) = 2\Omega (\alpha_{00}^2 + \alpha_{20}^2 + 2\alpha_{22}^2). \quad (25)$$

In order to solve Eq. (24), the constraint of the fixing valence nucleon number must be imposed. In the next subsection, we shall first calculate the Hamiltonian function, and then introduce several canonical transformations to eliminate this constraint.

A. The Hamiltonian function of the $\text{Sp}(6)$ model

The expectation value of the Hamiltonian operator (1) in the ICS is defined by

$$\langle \hat{H} \rangle = \epsilon \langle \hat{n} \rangle + G_0 \langle \hat{S}^+ \hat{S} \rangle + b_2 \sum_{l=1,2} \langle \hat{P}_l \cdot \hat{P}_l \rangle. \quad (26)$$

The detailed form will be given later. Since the valence nucleon number is conservative, the first term in Eq. (26) can be removed. Hence, Eq. (26) can be simplified as

$$\langle \hat{H} \rangle = E_{[\text{SU}(2)]} + E_{[\text{SU}(3)]}, \quad (27)$$

with

$$\begin{aligned} E_{[\text{SU}(2)]} &= G_0 \langle \hat{S}^+ \hat{S} \rangle, \\ E_{[\text{SU}(3)]} &= b_2 \sum_{l=1,2} \langle \hat{P}_l \cdot \hat{P}_l \rangle, \end{aligned} \quad (28)$$

where the coherent state expectation values can be explicitly calculated in ICS,

$$\begin{aligned}
\langle \hat{S}^+ \hat{S} \rangle &= \frac{\Omega}{3} \left(\frac{n}{2} + \left(1 - \frac{\Omega}{3}\right) K_2 + \frac{2\Omega}{3} K_1 \right), \\
\langle \hat{P}_1 \cdot \hat{P}_1 \rangle &= \frac{3n}{4} - \frac{\Omega}{2} K_3 - \frac{\Omega}{2} K_1, \\
\langle \hat{P}_2 \cdot \hat{P}_2 \rangle &= \frac{7n}{4} - \frac{3n^2}{4\Omega} + \frac{\Omega}{2} K_1 + \frac{\Omega}{3} K_2 \left(\frac{2}{3} - 1 \right) + \frac{\Omega}{3} K_3 \left(\frac{1}{2} - \frac{2\Omega}{3} \right),
\end{aligned} \tag{29}$$

and

$$\begin{aligned}
K_1 &= \frac{1}{2} \sum_{i \neq j} \left[\sqrt{1 - |S_i|^2} \sqrt{1 - |S_j|^2} S_i S_j^* \right], \\
K_2 &= \sum_i |S_i|^4, \\
K_3 &= \frac{1}{2} \sum_{i \neq j} \left[|S_i|^2 |S_j|^2 \right].
\end{aligned} \tag{30}$$

In Appendix B, we have shown that the Sp(6) model in this parameter representation (quantum phase space) contains all the general properties of the nuclear geometrical model [14].

B. The semiquantal dynamical equations without constraint in the Sp(6) model

To remove the constraint of the fixed valence nucleon number, several canonical transformations have to be made. Let the complex variables $S_i = q_i + ip_i$, where q_i and p_i are real variables. The Hamilton-like equation (24) can then be reexpressed as:

$$\begin{aligned}
\frac{2\Omega}{3} \dot{p}_i &= -\frac{\partial \langle \hat{H} \rangle}{\partial q_i}, \\
\frac{2\Omega}{3} \dot{q}_i &= \frac{\partial \langle \hat{H} \rangle}{\partial p_i}, \quad i = x, y, z,
\end{aligned} \tag{31}$$

where the Planck constant \hbar has been absorbed into the Hamiltonian function. Next, we introduce a canonical transformation to generate the new canonical variables $\{\mathcal{P}_i, \mathcal{Q}_i\}$, and choose the second type generating functions as

$$\begin{aligned}
F_1^{(2)} &= \sum_{i=x,y,z} (f_i(+)) \text{ or } f_i(-), \\
f_i(+)) &= \frac{q_i}{2} \sqrt{\mathcal{P}_i^2 - q_i^2} + \frac{\mathcal{P}_i^2}{2} \left(\sin^{-1} \frac{q_i}{\mathcal{P}_i} - \frac{\pi}{2} \right), \\
f_i(-)) &= -\frac{q_i}{2} \sqrt{\mathcal{P}_i^2 - q_i^2} + \frac{\mathcal{P}_i^2}{2} \left(\cos^{-1} \frac{q_i}{\mathcal{P}_i} \right).
\end{aligned} \tag{32}$$

This type of generating functions has eight assembles corresponding to positive or negative p_i , $i = x, y, z$. To be explicit, let us consider the special case, $F_1^{(2)} = \sum_i f_i(+)$. From this canonical transformation, we can find the connections between the new and odd canonical variables,

$$\begin{aligned} p_i &= \frac{\partial F_1^{(2)}}{\partial q_i} = \sqrt{\mathcal{P}_i^2 - q_i^2}, \\ \mathcal{Q}_i &= \frac{\partial F_1^{(2)}}{\partial \mathcal{P}_i} = \mathcal{P}_i \left(\sin^{-1} \frac{q_i}{\mathcal{P}_i} - \frac{\pi}{2} \right), \end{aligned} \quad (33)$$

or

$$\begin{aligned} q_i &= \mathcal{P}_i \cos \frac{\mathcal{Q}_i}{\mathcal{P}_i}, \\ p_i &\equiv |\mathcal{P}_i \sin \frac{\mathcal{Q}_i}{\mathcal{P}_i}|. \end{aligned} \quad (34)$$

This transformation is valid only for positive p_i . In another case $F_1^{(2)} = \sum_i f_i(-)$, one can get the same transformation but for negative p_i . This is because in this case $p_i = -\sqrt{\mathcal{P}_i^2 - q_i^2} = -|\mathcal{P}_i \sin \frac{\mathcal{Q}_i}{\mathcal{P}_i}|$ and $q_i = \mathcal{P}_i \cos \frac{\mathcal{Q}_i}{\mathcal{P}_i}$. All the eight generating functions transform the old variables $(p_x, p_y, p_z) = (+, +, +)$ or $(+, +, -)$ or $(-, -, +)$... into new variables $(\mathcal{P}_x, \mathcal{P}_y, \mathcal{P}_z)$, where $(+, +, +)$ means that p_x, p_y and p_z are all positive. Their connections to the variables S_i are given by

$$q_i^2 + p_i^2 = |S_i|^2 = \mathcal{P}_i^2, \quad (35)$$

and

$$S_i = q_i + ip_i = \mathcal{P}_i \exp \left(-i \frac{\mathcal{Q}_i}{\mathcal{P}_i} \right). \quad (36)$$

Note that Eq. (36) implies $\mathcal{P}_i \neq 0$ (if $\mathcal{Q}_i \neq 0$). In other words, the trajectories $(\mathcal{P}_x, \mathcal{P}_y, \mathcal{P}_z)$ cannot go through the section $\mathcal{P}_i = 0$. Therefore we have eight types of independent initial conditions, namely, $(\mathcal{P}_x, \mathcal{P}_y, \mathcal{P}_z) \in \{(\pm, \pm, \pm)\}$. Next, we will make the second canonical transformation. It transforms $(\mathcal{P}_i, \mathcal{Q}_i)$ into (P_i, Q_i) such that Q_z becomes an ignorable coordinate. We choose the second type generating function as

$$F_2^{(2)} = Q_x P_x + Q_y P_y \pm Q_z \sqrt{P_z^2 - P_x^2 - P_y^2}. \quad (37)$$

The connections between new and old variables are

$$\begin{aligned} \mathcal{P}_i &= \frac{\partial F_2^{(2)}(\pm)}{\partial Q_i} = P_i \quad , \quad i = x, y, \\ \frac{Q_z}{\mathcal{P}_z} &= \frac{Q_z}{\mathcal{P}_z} \quad , \quad \frac{Q_i}{\mathcal{P}_i} = \frac{Q_i}{\mathcal{P}_i} - \frac{Q_z}{\mathcal{P}_z} \quad , \quad i = x, y, \\ \mathcal{P}_z^2 &= P_z^2 - P_x^2 - P_y^2 \quad \text{or} \quad P_z^2 = \sum_i |S_i|^2 = \frac{3n}{2\Omega}. \end{aligned} \quad (38)$$

By using these two steps of transformations, the relations between two sets of canonical variables $\{S_i, S_i^*\}$ and $\{P_i, Q_i\}$ are given by

$$\begin{aligned} |S_i|^2 &= P_i^2 \quad , \quad i = x, y, \\ |S_z|^2 &= \frac{3n}{2\Omega} - P_x^2 - P_y^2, \\ S_x S_y^* &= P_x P_y \exp \left[-i \left(\frac{Q_x}{P_x} - \frac{Q_y}{P_y} \right) \right], \\ S_i S_z^* &= P_i \sqrt{\frac{3n}{2\Omega} - P_x^2 - P_y^2} \exp \left(-i \frac{Q_i}{P_i} \right), \quad i = x, y. \end{aligned} \quad (39)$$

The Hamiltonian function H can be expressed now in terms of (P_x, P_y, Q_x, Q_y) :

$$\begin{aligned} H \equiv \langle \hat{H} \rangle &= b_2 \left(\frac{5n}{2} + \frac{n^2}{2} - \frac{3n^2}{2\Omega} \right) + G_0 \left(-\frac{n^2}{4} + \frac{3n^2}{4\Omega} + \frac{n\Omega}{6} \right) \\ &+ \left(b_2 \frac{1-2\Omega}{3} + G_0 \frac{2(\Omega-3)}{9} \right) H_1 + G_0 \frac{2\Omega^2}{9} H_2, \end{aligned} \quad (40)$$

where

$$H_1 = \frac{3n}{2} (P_x^2 + P_y^2) - \Omega (P_x^4 + P_y^4 + P_x^2 P_y^2), \quad (41)$$

$$\begin{aligned} H_2 &= \sqrt{(1-P_x^2)(1-\mathcal{P}_z^2)} P_x \mathcal{P}_z \cos \left(\frac{Q_x}{P_x} \right) \\ &+ \sqrt{(1-P_y^2)(1-\mathcal{P}_z^2)} P_y \mathcal{P}_z \cos \left(\frac{Q_y}{P_y} \right) \\ &+ \sqrt{(1-P_x^2)(1-P_y^2)} P_x P_y \cos \left(\frac{Q_x}{P_x} - \frac{Q_y}{P_y} \right), \end{aligned} \quad (42)$$

with

$$\mathcal{P}_z = \sqrt{\left(\frac{3n}{2\Omega} - P_x^2 - P_y^2 \right)}. \quad (43)$$

The new Hamilton-like equations become

$$\begin{aligned}\frac{2\Omega}{3}\dot{P}_i &= -\frac{\partial H}{\partial Q_i}, \\ \frac{2\Omega}{3}\dot{Q}_i &= \frac{\partial H}{\partial P_i}, \quad i = x, y.\end{aligned}\tag{44}$$

Note that the 3rd canonical momentum P_z is a conservative quantity because Q_z is an ignorable coordinate (i.e., it does not appear in the Hamiltonian function). Therefore, the quantum phase space of nuclear deformation is reduced to a four-dimensional space after solving the constraint of the fixing valence nucleon number. Thus, we have formulated the semiquantal dynamics of the Sp(6) model in a four-dimensional quantum phase space, which determines the dynamical evolution of nuclear deformation.

IV. THE DYNAMICAL PAULI EFFECT AND CHAOTIC MOTION

A. Pauli forbidden region in (P_i, Q_i) -phase space

Although we have formulated the semiquantal dynamics of the Sp(6) model in a four-dimensional phase space, this phase space is still a nontrivial geometrical space. As we have seen in the previous section, this quantum phase space is a compact space. It is embedded in a four-dimensional flat space. Besides, due to the Pauli effect of the Sp(6) model [12], not the whole domain of this quantum phase space is dynamically allowed. When the valence nucleon number $n \geq \frac{2\Omega}{3}$, some region is forbidden due to the Pauli effect [15]. Explicitly, we can see from Appendix A that the diagonal submatrix block parameters \mathbf{Y} in the Sp(6) CS satisfy the condition $\mathbf{Y}^2 = \mathbf{1} - \mathbf{X}\mathbf{X}^+$. Consider the parameter space in the intrinsic frame. The matrix $\mathbf{Y}_{in} (= \pm \sqrt{\mathbf{1} - \mathbf{X}_{in}\mathbf{X}_{in}^+})$ has the form:

$$\mathbf{Y}_{in} = \pm \begin{pmatrix} \sqrt{1 - |S_x|^2} & 0 & 0 \\ 0 & \sqrt{1 - |S_z|^2} & 0 \\ 0 & 0 & \sqrt{1 - |S_y|^2} \end{pmatrix}.\tag{45}$$

Since the matrix \mathbf{Y}_{in} is hermitian, it means that $|S_i|^2 \leq 1$. Together with the condition of the fixing valence nucleon number, $\sum_i |S_i|^2 = \frac{3n}{2\Omega}$, we obtain the following conclusion: When $\Omega \geq n > \frac{2\Omega}{3}$ (or $\sum_k |S_k|^2 > 1$) [see Eq. (25)], the condition $|S_i| \leq 1$ is not satisfied for the whole domain. A forbidden region appears in the quantum phase space, and its contour plotted in $\alpha_{20} - \sqrt{2}\alpha_{22}$ plane can be determined by using Eq. (B2) [15]. When $n \leq \frac{2\Omega}{3}$ (or $\sum_k |S_k|^2 \leq 1$), the condition $|S_i| \leq 1$ is always satisfied so that there is no forbidden region in the phase space. Note that the critical value $n = \frac{2\Omega}{3}$ has an important consequence in the Sp(6) model. When $n \leq \frac{2\Omega}{3}$, the nuclear collective motions can be described in the symmetric representation of the subgroup SU(3) of Sp(6), which behaves the same as the bosonic SU(3) representation. However, when $\Omega \geq n > \frac{2\Omega}{3}$, the Pauli principle forces the system to move to an asymmetric representation of SU(3). Correspondingly, the nuclear deformation will be limited in the quantum phase space. The condition $|S_i| \leq 1$ is indeed such a phase space constraint of the Pauli effect in the Sp(6) model [15].

In conclusion, within the constraint of the fixing valence nucleon number and the presence of the Pauli effect, the quantum phase space of the Sp(6) model is only a limited domain in a four-dimensional flat space restricted by $\frac{3n}{2\Omega} - P_x^2 - P_y^2 \geq 0$ and $1 - |S_i|^2 \geq 0$. This is a pure quantum mechanical effect on geometry. In the following, we shall explore the dynamical consequence of these quantum effects to the chaotic motions.

B. Analysis of chaotic motion in the Sp(6) model

In this subsection, we shall numerically analyze the chaotic motion in the Sp(6) model. Since the semiquantal dynamics is determined by the Hamilton-like equations of motion (44), the chaos can be described in terms of Poincare' surface of section (PSS). We will first examine the nuclear surface motions in the dynamical symmetry limits of the Sp(6) model. The Hamiltonian in the intrinsic frame can be expressed as:

$$\begin{aligned}
 H &= G_0 \langle \hat{S}^+ \hat{S} \rangle + b_2 \sum_{l=1,2} \langle \hat{P}_l \cdot \hat{P}_l \rangle \\
 &\equiv T_{eff}(\alpha_{\lambda\mu}, \pi_{\lambda\mu}) + V_{eff}(\alpha_{\lambda\mu})
 \end{aligned}$$

$$= T_{eff}(P_i, Q_i) + V_{eff}(P_i), \quad (46)$$

where T_{eff} is an effective kinetic energy which contains the general kinetic energy and a velocity-dependent potential; and V_{eff} is an effective potential of the $\text{Sp}(6)$ model derived in Appendix B. In the intrinsic frame, the $\text{Sp}(6)$ model has two group chains: the $\text{SU}(2)$ chain (with $b_2 = 0$) and the $\text{SU}(3)$ chain (with $G_0 = 0$). These two limiting cases describe the nuclear vibrational mode and the γ -stable rotational mode, respectively. The numerical results of Fig. 1a and 1b shows that their PSS are regular. This is because the existence of dynamical symmetries in these two limits guarantees the integrability of dynamics [16]. However, when both G_0 and b_2 are not equal to zero, the above dynamical symmetries are broken and chaos appears. This is shown in Fig. 1c.

To demonstrate the chaotic behavior in the nuclear surface motions, we fix the rate G_0/b_2 and vary the particle number n to analyze the phase space structure of the semiquantal dynamics. There is a phase transition from the vibrational to the rotational modes in the nuclear surface motions. According to the result in Ref. [14], this phase transition is associated with the dynamical symmetry breaking from the $\text{SU}(2)$ to the $\text{SU}(3)$ limit with fixed G_0/b_2 , and taking n as the control parameter. Therefore, chaos must occur accompanied with this phase transition [16,17]. In the following numerical calculation, we take $G_0 = -.035$ MeV and $b_2 = -.065$ MeV with $\Omega = 36$. Note that the chaotic behavior also varies with the energy which can be regarded as a scale for analyzing the strength of chaotic motion.

The numerical results show that the patterns of PSS in the $\text{Sp}(6)$ model can be divided into three types with n increasing. For the cases of $n = 2 \sim 8$, the PSS have the ‘similar’ patterns with the energy increasing. We classify this type of PSS class A. The cases $n = 10 \sim 16$ form class B, and $n = 18 \sim 36$ form class C. Here, the word ‘similar’ means that the PSS are topologically similar, namely, the PSS of two states have the similar type of KAM surfaces and the similar distribution of chaotic phase space structure. For example, in Fig. 2c and 2d, the state of $E = -6.8$ MeV with $n = 10$ is similar to the state of $E = -7.7$ MeV

with $n = 12$. Analogously, the state $E = -3.95$ MeV with $n = 10$ is similar to $E = -4$ MeV with $n = 12$, and $E = -3.4$ MeV with $n = 10$ is similar to $E = -3.5$ MeV with $n = 12$. Physically, this classification depends on the contribution rate of the quadrupole and the pairing interactions. Roughly speaking, class A corresponds to the states with pairing interaction dominating, class C with quadrupole interaction dominating, and class B is the mixed states. In Fig. 2, six special cases of the PSS are plotted. They show the differences of PSS among the classes A, B and C. These Poincare surfaces of section (with $Q_x = 0$) are plotted in the $\alpha_{20} - \alpha'_{22}$ plane ($\alpha'_{22} \equiv \sqrt{2}\alpha_{22}$), and have a $\gamma = \frac{\pi}{3}$ -axis symmetry.

In order to define chaotic strength in a uniform way, we rescale the time $t \rightarrow tV_{max}$ [$V_{max} = (\text{maximum of } |V_{eff}|)$] such that the minimum values of the allowed energy are rescaled to -1 for all the values of n . This rescaling does not change the structure of the corresponding PSS. Also, for convenience, we introduce three energy scales: E_u , E_w and E_s . The energy scale E_s is the starting energy of the strong quantum chaos, E_w the starting energy of the weak quantum chaos, and E_u the upper bound of energy within which the Sp(6) model dominates the low-lying nuclear dynamics. Thus, for a given nucleus, the dynamical behavior of physical states can be divided into three types of motions: The pure regular motion which exists in the energy range from -1 to E_w , the weak chaotic motion in the range of E_w to E_s , and the strong chaotic motion in the range of E_s to E_u . Recalling the ‘pattern classification’ of the chaotic behavior aforementioned, systems with different n in the same class have similar patterns of PSS. Thus, E_w , E_s and E_u are all n dependent. We plot the phase diagram of chaotic behavior in the nuclear surface motions in the $E-n$ plane in Fig. 3. The chaotic strength is obtained by comparing the values of E_s and E_w in different n .

From Fig. 3, we see that when $n=2$ and 4 (small n), the contribution of the quadrupole interaction ($b_2 \sum_{l=1,2} \langle \hat{P}^l \cdot \hat{P}^l \rangle$ in Eq. (26)) is much smaller than the pairing interaction ($G_0 \langle \hat{S}^+ \hat{S} \rangle$). This implies that the system is near in the $SU(2) \subset Sp(6)$ dynamical symmetry. Correspondingly, the nuclear surface motion is near-integrable. Hence, for small n , the nuclear deformation is regular in all the energy ranges, as shown in Fig. 3 where

$E_w \simeq E_s \simeq E_u$ for small n . This corresponds to class A. When n is near $\frac{2\Omega}{3}$, we find that the quadrupole interactions is dominant. The nuclei are approximately described by the $SU(3) \supset Sp(6)$ dynamical symmetry. As we can see from Fig. 3, E_w and E_s are far from the minimum energy -1 . Therefore the phase space is filled mostly by the regular motion as well (with $n = 18 \sim 24$). This corresponds to class C. When the particle number n is between 8 to 14, the pairing interaction and the quadrupole interactions compete against each other, and all the dynamical symmetries in the $Sp(6)$ model are broken. This is the transition (mixed) region from the vibration to rotation in nuclear collective motions. The chaotic motion is very strong as it is shown in Fig. 3. This corresponds to class B.

The most remarkable result we find in this study is in the region $\frac{2\Omega}{3} < n < \Omega$. Naively, when $n > \frac{2\Omega}{3}$, the quadrupole interaction should be dominant so that the system should approximately have the $SU(3)$ dynamical symmetry. However, the numerically result shown in Fig. 3 tells us that when n varies from $\frac{2\Omega}{3}$ to the middle shell ($\frac{\Omega}{2}$), the strength of chaotic dynamics is increased. This unusual result is indeed caused by the Pauli effect. The Pauli principle forces the system to jump from the symmetric $SU(3)$ representation to the antisymmetric $SU(3)$ representation when $n > \frac{2\Omega}{3}$. This reduces the nuclear deformation (inhibiting the quadrupole interaction and increasing pairing interaction). As a result, the system deviates away from the $SU(3)$ dynamical symmetry and therefore leads to the stronger chaos. This is the first example to dynamically examine the Pauli effect on chaos. It is also the first evidence of showing the enhancement of chaos in quantum system due to the Pauli principle.

V. SUMMARY

In this paper, the $Sp(6)$ model have been chosen as an example to examine the chaotic dynamics in quantum systems caused by dynamical symmetry breaking and dynamical Pauli effect. It has been tested for many systems where dynamical symmetry breaking is closely related to quantum chaos [3,16,17]. However, this is the first paper to address the problem

of Pauli effect on chaotic dynamics. Since Pauli effect is a pure quantum mechanical phenomenon and it has no classical limit, its influence on chaos is certainly an important key to understand the intrinsic mechanism of quantum chaos. In this paper, we only present the evidence of Pauli effect on chaos in a specific system. The most interesting and challenge questions are whether the dynamical Pauli effect can always enhance chaotic motions and what generic role does the Pauli principle play in nonlinear dynamics of quantum theory? We leave these questions for future investigations.

ACKNOWLEDGMENTS

We would like to acknowledge the discussions with D. H. Feng, H. T. Mo, Y. H. Wong, S. L. Lin and C. T. Li. We also thank S. P. Li for his careful reading of the manuscript. This work is supported by the Department of Physics of National Taiwan University under Grant 5010202-02-434 (MTL) and the National Science Council of the Republic of China under Grant NSC86-2816-M001-008L (WMZ).

APPENDIX A: SP(6) COHERENT STATES

To make this paper self-contained, we briefly list in this appendix the main results of the Sp(6) coherent states which has been discussed in Ref. [14]. The coherent states of the group USp(6) (the compact group of the Lie algebra Sp(6)) are defined by

$$|\eta\rangle = \hat{T}(\eta)|0\rangle, \quad (\text{A1})$$

where the generalized displacement operator $\hat{T}(\eta)$, the coset representative of USp(6)/U(3), is given by

$$\hat{T}(\eta) = \exp \left[\left(\eta_{00} \hat{S}^+ + \sum_{\mu} \eta_{2\mu} \hat{D}_{\mu}^+ \right) - H.C. \right], \quad (\text{A2})$$

and $|0\rangle$ is the core vacuum (nearest closed shell), \hat{S}^+ and \hat{D}_{μ}^+ the pair creation operators in the Sp(6) model. The matrix representation of $\hat{T}(\eta)$ has the form:

$$\hat{T}(\eta) \rightarrow \text{Rep}(\hat{T}) = \begin{bmatrix} \mathbf{Y} & \mathbf{X} \\ -\mathbf{X}^+ & \tilde{\mathbf{Y}} \end{bmatrix} \equiv \mathbf{T}, \quad (\text{A3})$$

where the matrices \mathbf{X} and \mathbf{Y} are the 3×3 subblock matrices of the coset representative of USp(6)/U(3). Their explicit forms are given by

$$\mathbf{X} = \begin{bmatrix} \sqrt{3}\chi_{22} & \sqrt{\frac{3}{2}}\chi_{21} & \chi_{00} + \sqrt{\frac{1}{2}}\chi_{20} \\ \sqrt{\frac{3}{2}}\chi_{21} & -\chi_{00} + \sqrt{2}\chi_{20} & \sqrt{\frac{3}{2}}\chi_{2-1} \\ \chi_{00} + \sqrt{\frac{1}{2}}\chi_{20} & \sqrt{\frac{3}{2}}\chi_{2-1} & \sqrt{3}\chi_{2-2} \end{bmatrix}, \quad (\text{A4})$$

where $\chi_{\lambda\mu}$ is a function of $\{\eta_{\lambda\mu}\}$. There are totally twelve parameters in this coherent state. Since the matrix \mathbf{T} is unitary, the matrix \mathbf{X} must be symmetric and the matrix \mathbf{Y} is hermitian and is determined by \mathbf{X} from the following relations:

$$\mathbf{Y}\mathbf{Y} + \mathbf{X}\mathbf{X}^+ = \mathbf{I}, \quad \mathbf{Y}\mathbf{X} = \mathbf{X}\tilde{\mathbf{Y}}. \quad (\text{A5})$$

APPENDIX B: GEOMETRICAL MODEL VIA THE SP(6) MODEL

In this appendix, the geometrical model and the Sp(6) model will be compared. Without any loss of generality, we define the nuclear surface variables as

$$\begin{aligned}\alpha_{20}(t) &= \beta(t) \cos[\gamma(t)] \quad , \\ \alpha_{22}(t) &= \frac{1}{\sqrt{2}}\beta(t) \sin[\gamma(t)] \quad ,\end{aligned}\tag{B1}$$

where $\beta(t)$ and $\gamma(t)$ are the usual geometrical deformation parameters. Substituting Eq. (B1) into Eq. (19), it gives

$$|S_i| = -\alpha_{00} + \sqrt{2}\beta \cos\left(\gamma - \frac{2k_i}{3}\pi\right) \quad ,\tag{B2}$$

where $i = z, x, y; k_z = 0, k_x = 1, k_y = 2$ and

$$-\alpha_{00} = \sqrt{\frac{n}{2\Omega} - \beta^2} \quad .\tag{B3}$$

The effective potential of the Sp(6) model is

$$V_{eff} = \langle \hat{H}(\pi_{00}, \pi_{20}, \pi_{22} = 0; \alpha_{00}, \alpha_{20}, \alpha_{22}) \rangle \quad ,\tag{B4}$$

where $\pi_{\lambda\mu}$ is the conjugate momentum of $\alpha_{\lambda\mu}$. When these variables are zero, the variables S_i in Eq. (19) become real (for a proof, see Appendix C). Substituting the real variables S_i of Eq. (B2) into Eqs. (28-29), the effective potential can be expressed as:

$$V_{eff[G]} = A\beta^4 + B\beta^2 + C\alpha_{00}\beta^3 \cos 3\gamma + D + F \quad .\tag{B5}$$

where the stiffness coefficients A, B, C, D and F are listed as follows: For $G = \text{SU}(2)$,

$$\begin{aligned}A &= 7\Omega(\Omega/3 - 1)/2 \quad , \quad B = -2n(\Omega/3 - 1) \quad , \\ C &= 2\sqrt{2}\Omega(\Omega/3 - 1) \quad , \quad D = n(\Omega - n/2 + 3n/(2\Omega))/6 \quad , \\ F &= (\Omega/3)^2 \sum_{i \neq j, i, j = x, y, z} S_i S_j \left[(1 - S_i^2) (1 - S_j^2) \right]^{1/2} \quad ,\end{aligned}\tag{B6}$$

and for $G = \text{SU}(3)$,

$$\begin{aligned}
A &= -7\Omega(2\Omega - 1)/4 \quad , \quad B = n(2\Omega - 1) , \\
C &= -\sqrt{2}\Omega(2\Omega - 1) \quad , \quad D = 5n(2\Omega - n)/(4\Omega) \quad , \quad F = 0 .
\end{aligned}
\tag{B7}$$

These results agree with that of Ref. [14]. The effective potential of the Sp(6) model also has the same form as the potential energy of the geometrical model in the intrinsic frame

$$V_{eff}[\beta, \gamma] = \frac{1}{5}C_4\beta^4 + \frac{1}{2}C_2\beta^2 - \sqrt{\frac{2}{35}}\beta^3 \cos 3\gamma + \dots
\tag{B8}$$

In other words, the Sp(6) model in this picture contains all the properties of the nuclear geometrical model.

APPENDIX C: DEFORMATION PHASE SPACE

In this appendix, we will show that the surface variables, α_{00}, α_{20} and α'_{22} and their conjugate momentum π_{00}, π_{20} and π'_{22} form the canonical variables, where $\alpha'_{22} \equiv \sqrt{2}\alpha_{22}$. To do so, we introduce the fourth type generating function

$$F^{(4)} = -\frac{\pi_{00}}{3} (\mathcal{P}_x + \mathcal{P}_y + \mathcal{P}_z) - \frac{\pi_{20}}{3\sqrt{2}} (\mathcal{P}_x + \mathcal{P}_y - 2\mathcal{P}_z) - \frac{\pi'_{22}}{\sqrt{6}} (\mathcal{P}_y - \mathcal{P}_x) .
\tag{C1}$$

It transforms the canonical variables $\{\mathcal{P}_i, \mathcal{Q}_i, i = x, y, z\}$ mentioned in Sec. III into another set of the variables $\{\alpha_{\lambda\mu}, \pi_{\lambda\mu}\}$. The connection between these two sets of variables are

$$\begin{aligned}
\mathcal{Q}_x &= -\frac{\partial F^{(4)}}{\partial \mathcal{P}_x} = \frac{1}{3} \left(\pi_{00} + \frac{\pi_{20}}{\sqrt{2}} - \sqrt{\frac{3}{2}}\pi'_{22} \right) , \\
\mathcal{Q}_y &= -\frac{\partial F^{(4)}}{\partial \mathcal{P}_y} = \frac{1}{3} \left(\pi_{00} + \frac{\pi_{20}}{\sqrt{2}} + \sqrt{\frac{3}{2}}\pi'_{22} \right) , \\
\mathcal{Q}_z &= -\frac{\partial F^{(4)}}{\partial \mathcal{P}_z} = \frac{1}{3} \left(\pi_{00} - \sqrt{2}\pi_{20} \right) ,
\end{aligned}
\tag{C2}$$

and $\alpha_{\lambda\mu} = \frac{\partial F^{(4)}}{\partial \pi_{\lambda\mu}}$ gives the same relation listed in Eq. (19). The explicit connection between the variables S_i and $(\alpha_{\lambda\mu}, \pi_{\lambda\mu})$ can be found by using $S_i = \mathcal{P}_i \exp(-i\frac{\mathcal{Q}_i}{\mathcal{P}_i})$. Hence $\{\alpha_{\lambda\mu}, \pi_{\lambda\mu}\}$ are the canonical variables. Eq. (C2) and $S_i = \mathcal{P}_i \exp(-i\frac{\mathcal{Q}_i}{\mathcal{P}_i})$ imply that S_i is real when $\pi_{\lambda\mu} = 0$. Thus we can easily obtain the effective potential discussed in Appendix B.

REFERENCES

- [1] O. Bohigas, in “Chaos and Quantum Systems”, Proc. NATO ASI Les Houches Summer School, Eds. M. J. Giannoni, A. Voros and J. Zinn-Justin, (Amsterdam, Elsevier, 1991).
- [2] M. Gutzwiller, “Chaos in Classical and Quantum Mechanics”, (Springer-Verlag, 1990).
- [3] W. M. Zhang and D. H. Feng, *Phys. Rep.* **252**, 1–100 (1995).
- [4] W. M. Zhang, D. H. Feng, J. M. Yuan, Q. Pan, and T. Jjon, *Phys. Rev. A* **42**, 3646 (1990); W. M. Zhang and D. H. Feng, *J. Mod. Phys.* **A8**, 1417 (1993).
- [5] W. M. Zhang and M. T. Lee, “A simple picture of quantum suppression of chaos”, Preprint of Institute of Physics, Academia Sinica, Taiwan.
- [6] A. K. Pattanayak and W. C. Schieve, *Phys. Rev. Lett.* **72**, 2855 (1994).
- [7] B. Hu, B. Li and W. M. Zhang, “The quantum Frenkel- Kontorova Model, a squeezed state approach”, submitted to *Phys. Rev. Lett.* (1997).
- [8] B. Hu, B. Li, J. Liu, and J. Zhou, “Quantum fluctuation: suppression or enhancement of chaos”, submitted to *Phys. Rev. Lett.* (1997).
- [9] W. M. Zhang, D. H. Feng, and R. Gilmore, *Rev. Mod. Phys.* **62**, 867 (1990).
- [10] W. M. Zhang, D. H. Feng and J. M. Yuan, *Phys. Rev. A* **42**, 7125 (1990).
- [11] C.-L. Wu, D. H. Feng, X.-G. Chen, J.-Q. Chen, and M. W. Guidry, *Phys. Rev. C* **36**, 1157 (1987); C.-L. Wu, D. H. Feng, and M. W. Guidry, *Adv. Nulc. Phys. Vol.* **21**, 227 (1995).
- [12] D, H. Feng, C.-L. Wu, M. W. Guidry, and Z. P. Li, *Phys. Lett. B* **205**, 156 (1988).
- [13] A. Bohr and B. R. Mottelson, “Nuclear Structure”, Vol. **2**, (Benjamin, New York, 1975).
- [14] W. M. Zhang, C.-L. Wu, D. H. Feng, J. N. Ginocchio, and M. W. Guidry, *Phys. Rev. C* **38**, 1475 (1988).

- [15] W. M. Zhang, D. H. Feng, C.-L. Wu, and M. W. Guidry, J. Phys. G **15**, L **115** (1989).
- [16] W. M. Zhang, C. C. Martens, D. H. Feng, and J. M. Yuan, Phys. Rev. Lett. **61**, 2167 (1988); W. M. Zhang, D. H. Feng, J. M. Yuan, and S. J. Wang, Phys. Rev. A **40**, 438 (1989).
- [17] W. M. Zhang, and D. H. Feng, Phys. Rev. C **43**, 1127 (1991).

FIGURES

FIG. 1. The Poincare surface of section ($Q_x = 0$) of the Sp(6) model with $\Omega = 36$, $n = 10$ and $E = -3.0$ MeV: (a) $G_0 = -0.1$ MeV, $b_2 = 0.$ MeV, (b) $G_0 = 0.$ MeV, $b_2 = -.1$ MeV, (c) $G_0 = -0.01$ MeV, $b_2 = -.09$ MeV.

FIG. 2. The Poincare surface of section ($Q_x = 0$) of the Sp(6) model with energy increasing, where $\Omega = 36$, $G_0 = -.035$ MeV, $b_2 = -.065$ MeV: (a) $n = 4$, (b) $n = 8$, (c) $n = 10$, (d) $n = 12$, (e) $n = 24$, (f) $n = 30$.

FIG. 3. A phase diagram of chaotic patterns in $E - n$ plane in the Sp(6) model with $\Omega = 36$, where R means the regular region, W the weak-chaotic region, and S the strong-chaotic region.

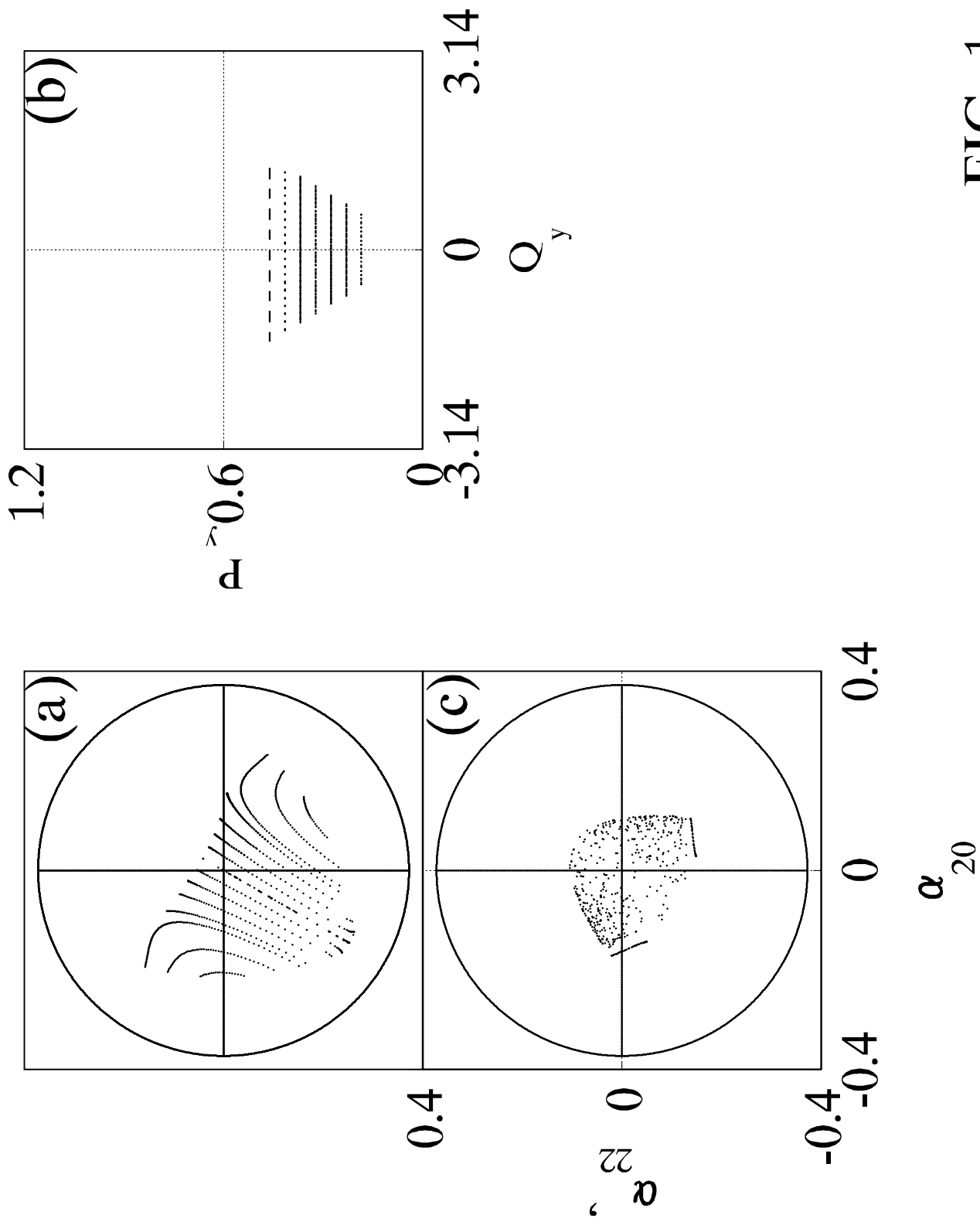


FIG. 1.

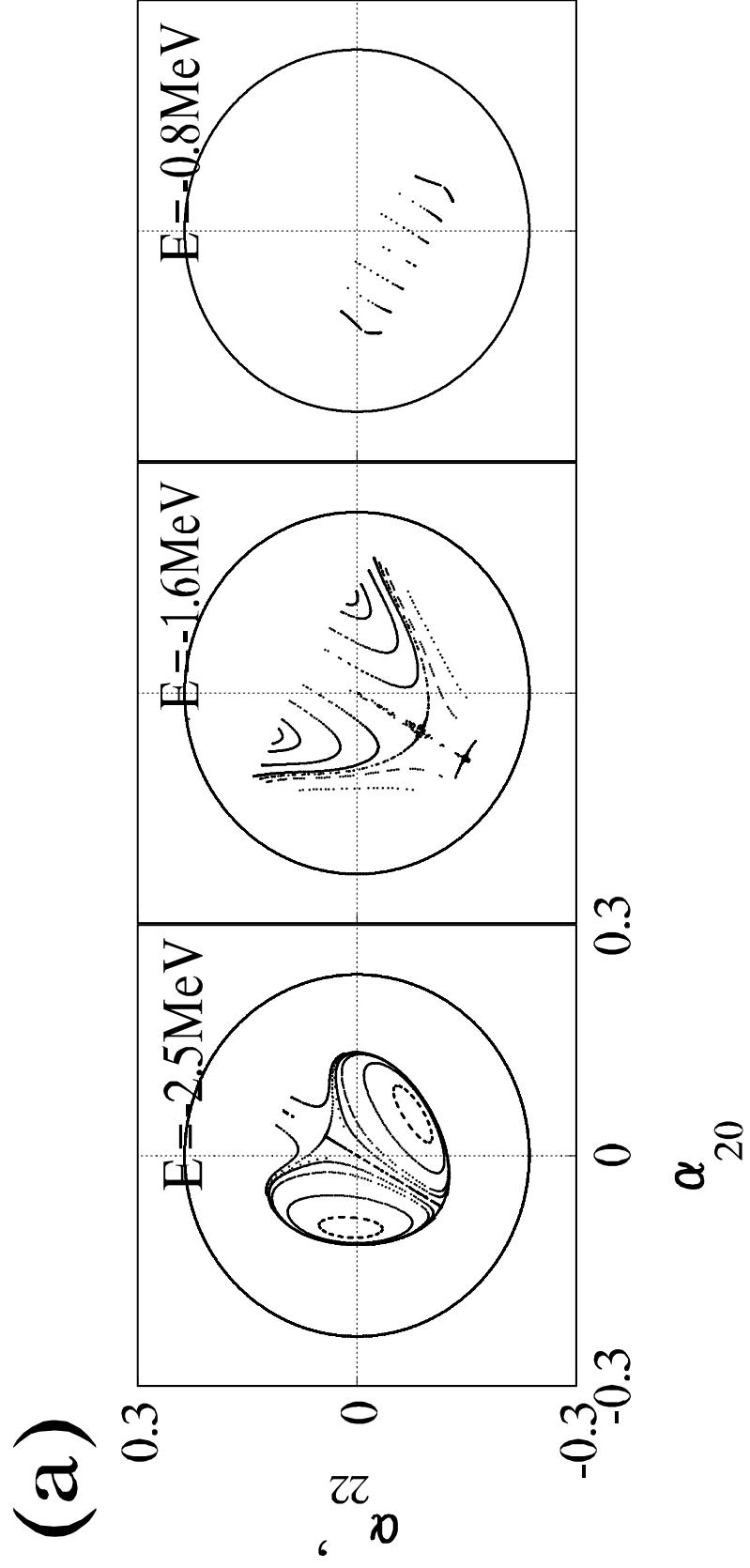


FIG. 2. (a)

(b)

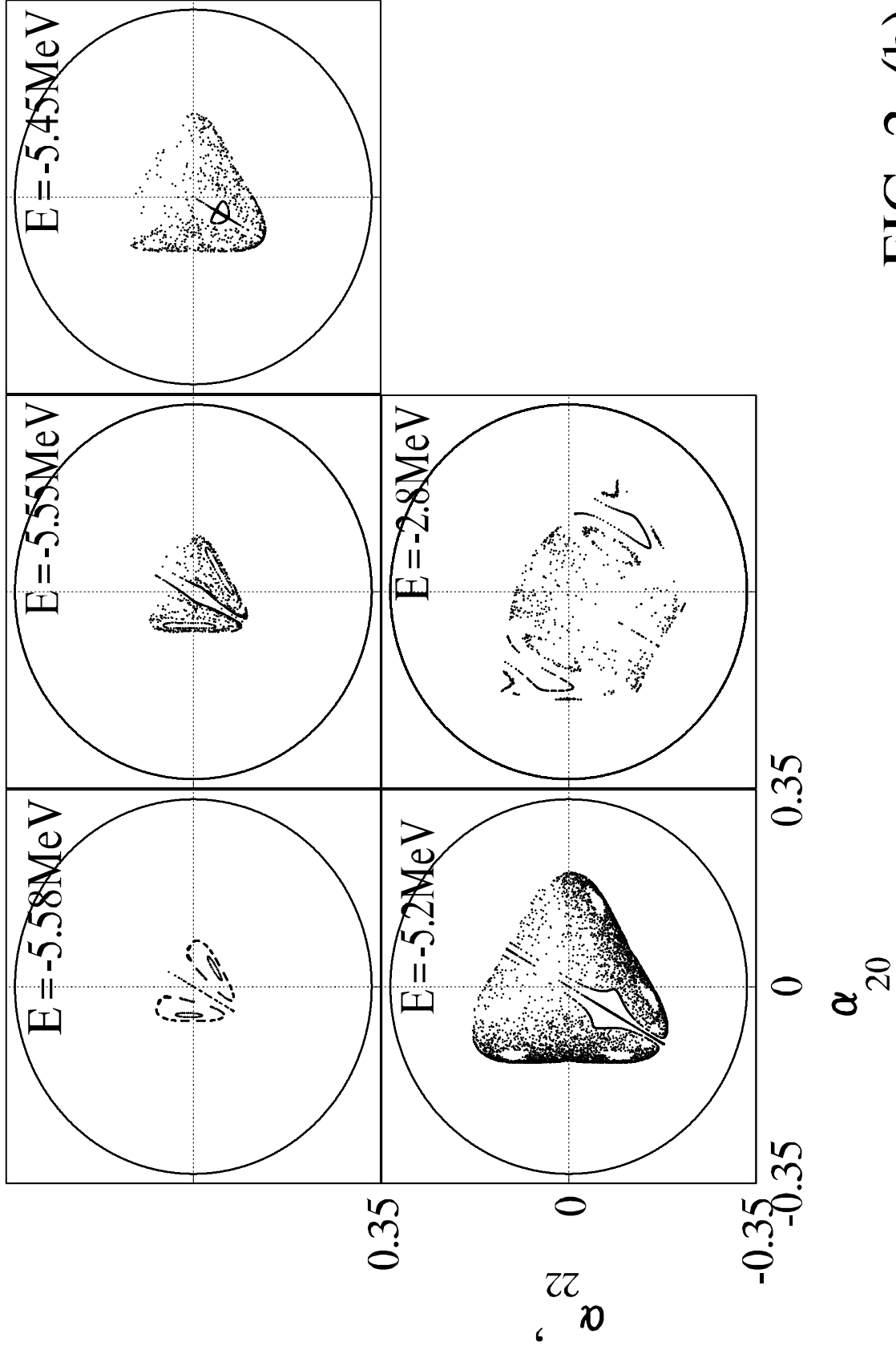


FIG. 2. (b)

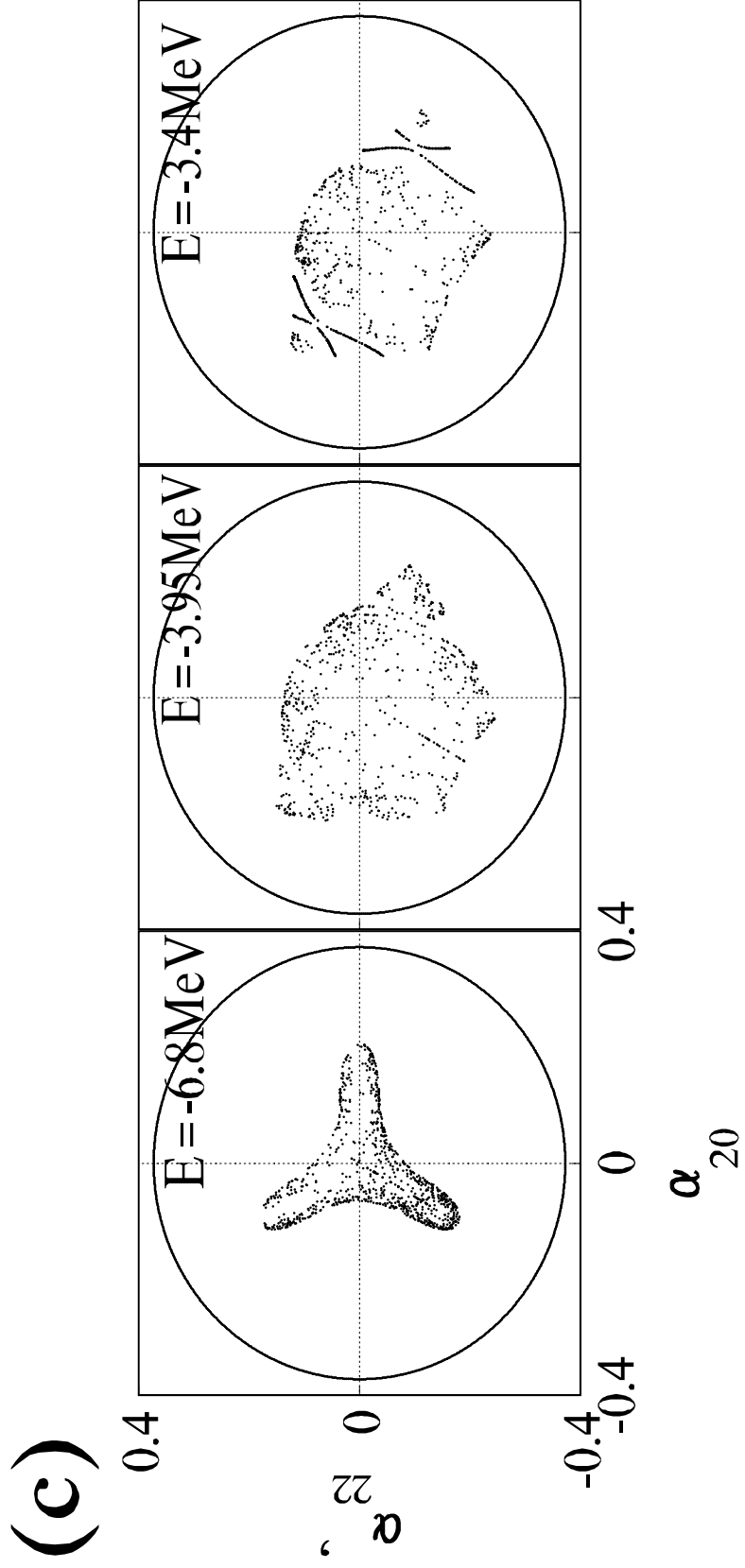


FIG. 2. (c)

(d)

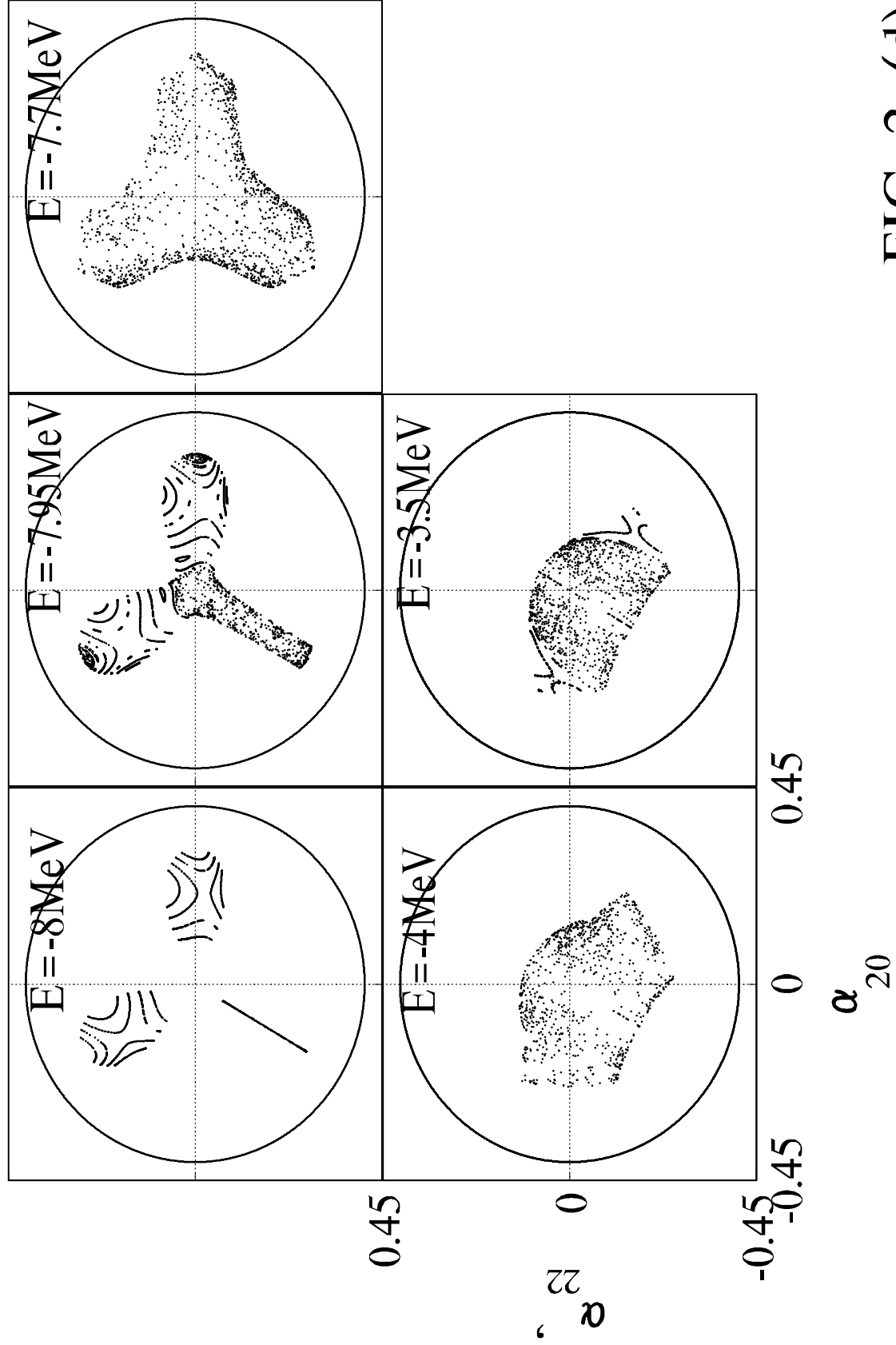


FIG. 2. (d)

(e)

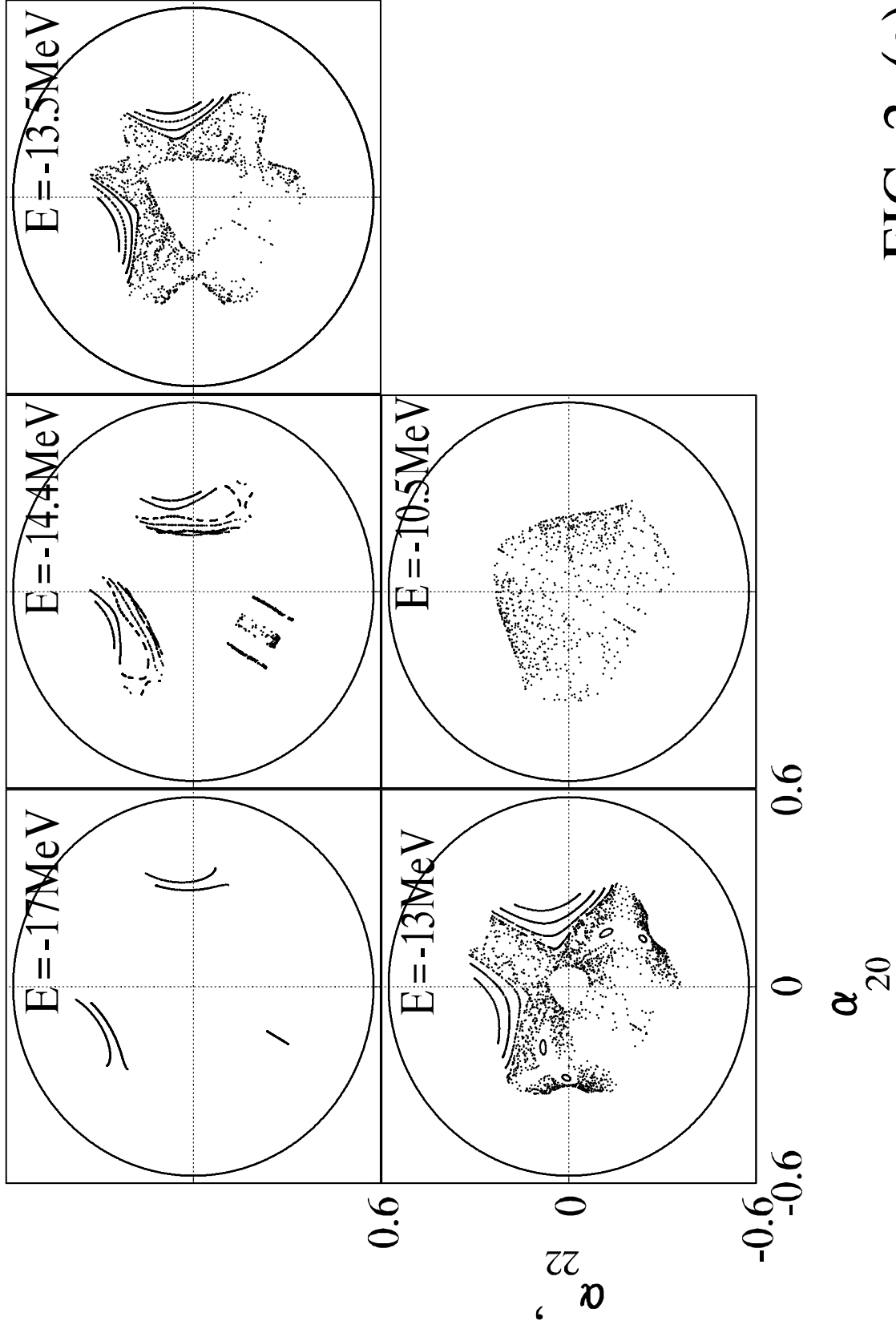


FIG. 2. (e)

(f)

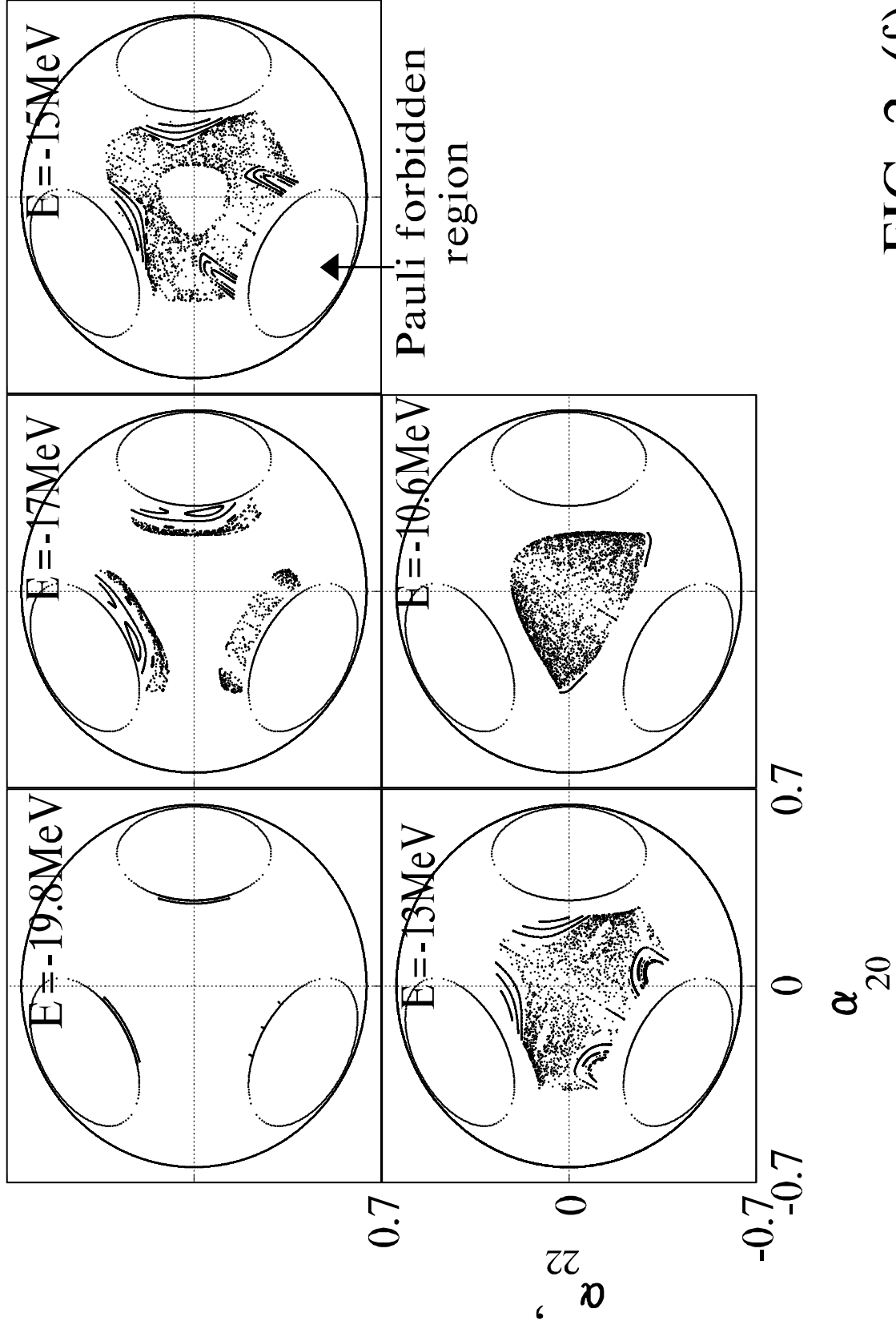


FIG. 2. (f)

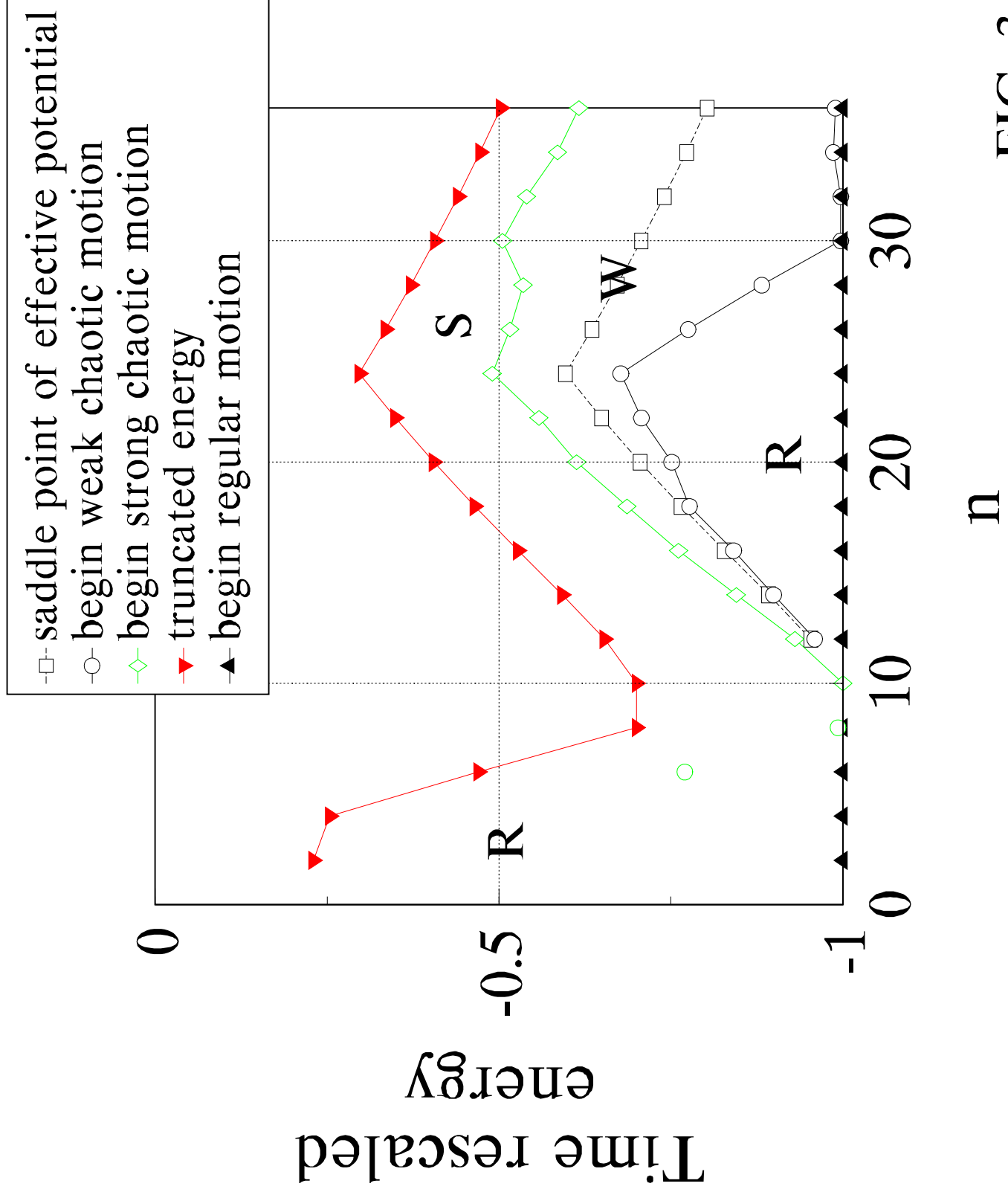


FIG. 3.